ACS Photonics

Article

pubs.acs.org/journal/apchd5

First-Principles Evaluation of the Alkali and/or Alkaline Earth Beryllium Borates in Deep Ultraviolet Nonlinear Optical Applications

Xingxing Jiang,[†,∥] Siyang Luo,[†] Lei Kang,[†,∥] Pifu Gong,[†,∥] Hongwei Huang,[‡] Shichao Wang,[*,§] Zheshuai Lin,[*,†] and Chuangtian Chen[†]

[†]Center for Crystal R&D, Key Lab of Functional Crystals and Laser Technology of Chinese Academy of Sciences, Technical Institute of Physics and Chemistry, CAS, Beijing 100190, China

[‡]School of Materials Science and Technology, China University of Geosciences, Beijing 100083, China

[§]Department of Chemistry, Northwestern University, Evanston, Illinois 60208, United States

[∥]University of Chinese Academy of Science, Beijing 100049, China

Supporting Information

ABSTRACT: The prospects of all known noncentrosymmetric alkali and/or alkaline earth beryllium borates for nonlinear optical (NLO) generation in the deep-ultraviolet (DUV) spectral region are evaluated by first-principles studies. It is shown that all these crystals possess large enough energy band gaps and relatively strong NLO responses that satisfy the requirement for DUV second-harmonic generation (SHG). However, the practical DUV SHG capabilities of these crystals are mostly limited by the phase-matching condition, as determined not only by the optical birefringence but also by the refractive-index dispersion that is explicitly emphasized for the first time in this work. Therefore, although the $K_2Be_2BO_3F$ family and $NaBeB_3O_6$ both have a large birefringence, $\Delta n \approx 0.08$, at a wavelength of 400 nm, the DUV SHG lasers can only be produced in the former but cannot be fulfilled in the latter due to its large refractive-index dispersion in the DUV region. The crystal structural features for large birefringence and the electronic structure origins for different refractive-index dispersion behaviors are discussed. The elucidation of the structure−property relationship presents a useful guide to the exploration of new NLO crystals that can be practically applied for DUV SHG.

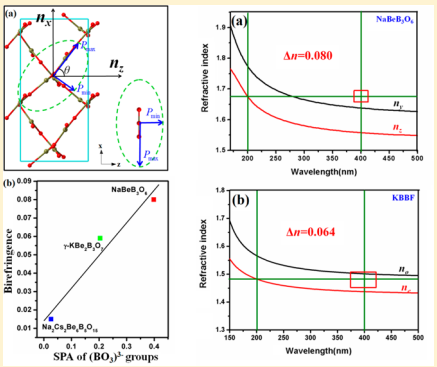

KEYWORDS: *alkali and/or alkaline earth beryllium borates, deep ultraviolet nonlinear optical, phase-matching condition, birefringence, refractive-index dispersion*

The demand for deep-ultraviolet (DUV, wavelength λ < 200 nm) coherent light becomes increasingly urgent, owing to its great application in many scientific and technical fields, such as in microcircuit photolithography, high density storage, laser micromachining, and high-precision scientific equipment.[1−5] Up to now, the most effective method to produce DUV lasers with high quality is from all-solid-state lasers using cascaded frequency conversion by DUV nonlinear optical (NLO) crystals.[6−9] The search for new NLO crystals for the DUV spectral region is one of the research hot spots in optoelectronic functional materials.[10−15]

It is commonly accepted that the following conditions of optical properties are vital for the DUV NLO performance of a crystal:[16,17] (i) a short-wavelength absorption cutoff (λ_{cutoff}) of less than 200 nm (i.e., an energy band gap E_g > 6.2 eV) for good optical transmission in the DUV region (also corresponding to a large laser damage threshold[18]); (ii) a relatively large second-harmonic-generation (SHG) response (usually the effective SHG effect should be larger than that of KH_2PO_4 (KDP, d_{36} = 0.39 pm/V)) for a high NLO conversion efficiency, and (iii) a moderate birefringence (Δn should be larger than 0.075 but smaller than 0.11 at a wavelength of 400 nm) for the achievement of the phase-matching condition in the DUV region.

For decades, the exploration of DUV NLO crystals has been focused on the noncentrosymmetric alkali and/or alkaline earth beryllium borates,[7−17] mainly due to their very short absorption edges and relatively large NLO effects. In the middle of the 1990s Chen's group discovered that the $KBe_2BO_3F_2$ (KBBF) crystal possesses an absorption cutoff wavelength of 150 nm and SHG coefficient of $d_{11} \approx 0.5$ pm/V, manifesting its good prospects for DUV laser generation.[19] Further investigations revealed that this crystal can produce DUV coherent light at 161 nm by direct SHG,[20] thus becoming the most important DUV NLO crystal. At the beginning of this century, the other two members in the KBBF family, $RbBe_2BO_3F_2$ (RBBF)[21] and $CsBe_2BO_3F_2$ (CBBF),[22] were discovered, and both of them also exhibit good DUV NLO performances. However, due to the strong layered tendency, the KBBF family is difficult to grow in

Received: May 7, 2015
Published: July 27, 2015

DOI: 10.1021/acsphotonics.5b00248
ACS Photonics 2015, 2, 1183−1191

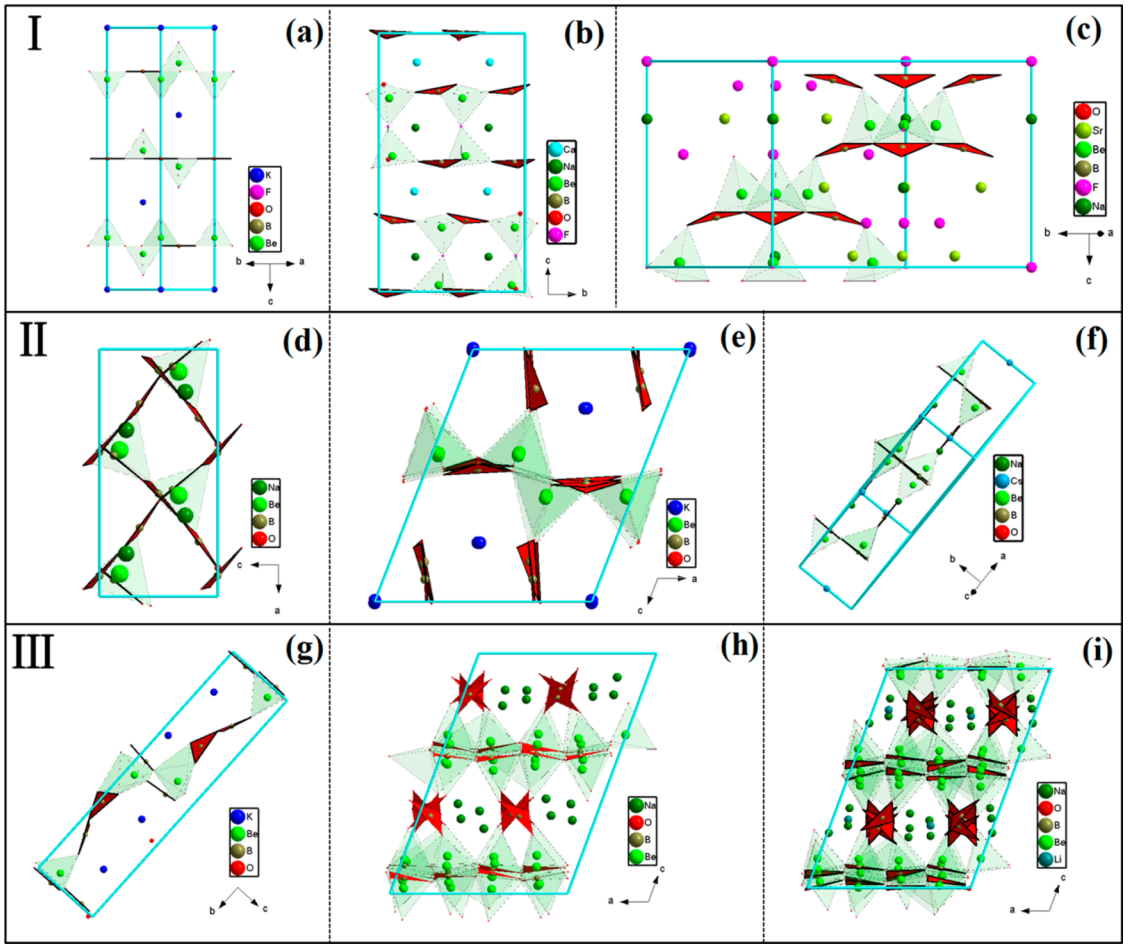

Figure 1. Unit cell for all known alkaline and/or alkaline earth beryllium borates. Here the structures are catalogued according to the arrangement of $(BO_3)^{3-}$ groups: in a nearly coplanar pattern (type-I), including (a) KBBF family crystals (KBBF, RBBF, and CBBF), (b) $NaCaBe_2B_2O_6F$, and (c) $NaSr_3Be_3B_3O_9F_4$; in a coaxial pattern (type-II), including (d) $NaBeB_3O_6$, (e) γ-$KBe_2B_3O_7$, and (f) $Na_2Cs_2Be_6B_5O_{15}$; and in other inclined patterns (type-III), including (g) β-$KBe_2B_3O_7$ and $RbBe_2B_3O_7$, (h) $Na_2Be_4B_4O_{11}$, and (i) $LiNa_5Be_{12}B_{12}O_{33}$. The $(BO_3)^{3-}$ and $(BeO_4)^{6-}$ (or $(BeO_3F)^{5-}$) groups are represented by red triangles and transparent green tetrahedra, respectively.

thick crystals; thus their practical applications are seriously hindered. Therefore, great efforts have been made to search for and design novel DUV NLO beryllium borates.

Up to now, a total of 13 new alkali and/or alkaline earth NLO beryllium borates have been discovered[20−27] (note $Sr_2Be_2B_2O_7$[28] is not considered in this work owing to its structural uncertainty[29]). In these crystals, the $(BO_3)^{3-}$ and $(BeO_4)^{6-}$ (or $(BeO_3F)^{5-}$) groups are connected to each other by sharing oxygen atoms, forming a three-dimensional (3D) framework or two-dimensional (2D) layers, and the alkali (or alkaline earth) cations are located in the interstices, as displayed in Figure 1. All these crystals were claimed to be very promising materials for DUV NLO applications. However, due to the difficulty of obtaining crystals with a large size and high optical quality, for most of these borates only the very basic optical properties, including the UV absorption edge from synthesized compounds (but not from single crystals) and the powder SHG effect, have been determined,[23−27] which provide only an approximation of their DUV SHG capability. For the same reason the birefringence (and refractive indices) of most of the materials has not been determined yet. Therefore, the real prospects of practical NLO applications for alkali and/or alkaline earth beryllium borates in the DUV region still remain unclear.

Due to the rapid development of the computational methodology and facilities, the linear and nonlinear optical properties of UV borates can be well predicted by first-principles calculations,[11,30−32] especially based on the density functional theory (DFT). Thus, the *ab initio* materials simulations have the capability to predict whether a newly discovered compound has the potential to be a good NLO crystal, so as to determine whether further experimental investigations, such as single-crystal growth and precise optical measurements, should be performed or not. This research approach can not only significantly improve the exploration efficiency but also greatly help experiments to save huge human and raw material resources. In this work, using first-principles calculations, the linear and nonlinear optical properties, including the energy band gaps, SHG coefficients, birefringence, and refractive indices for the alkali and/or alkaline earth NLO beryllium borates are determined. On the basis of the conditions for the DUV NLO performance, the application prospects of these crystals in the UV and DUV regions are systematically evaluated. In particular, the important role of refractive-index dispersion in determining the phase-matching condition is emphasized for the first time. The intrinsic relationship between property and structure (including atomic geometries and electronic structures) is discussed.

DOI: 10.1021/acsphotonics.5b00248
ACS Photonics 2015, 2, 1183−1191

Table 1. Calculated and Measured Band Gaps (eV) of the Investigated Beryllium Borate Crystals

	$KBe_2BO_3F_2$	$RbBe_2BO_3F_2$	$CsBe_2BO_3F_2$	$NaCaBe_2B_2O_6F$	$NaSr_3Be_3B_3O_9F$	$NaBeB_3O_6$
LDA	5.90	8.23	8.23	5.08	5.64	4.70
PBE0	8.30(150 nm)	8.25(150 nm)	8.25(150 nm)	7.04(176 nm)	7.31(170 nm)	7.29(170 nm)
expt	8.46(147 nm)	8.18(152 nm)	8.23(151 nm)	6.64[25](185 nm)	6.92[23](180 nm)	−(<200 nm)
	$Na_2Cs_2Be_6B_5O_{15}$	β-$KBe_2B_3O_7$	γ-$KBe_2B_3O_7$	$RbBe_2B_3O_7$	$Na_2Be_4B_4O_{11}$	$LiNa_5Be_{12}B_{12}O_{33}$
LDA	4.42	4.01	4.22	3.90	5.03	5.04
PBE0	6.49(192 nm)	6.65(187 nm)	6.70(186 nm)	6.95(179 nm)	6.88(181 nm)	7.30(171 nm)
expt	−(<200 nm)	−(<200 nm)	−(<200 nm)	−(<200 nm)	7.27[24](170 nm)	7.36[24](169 nm)

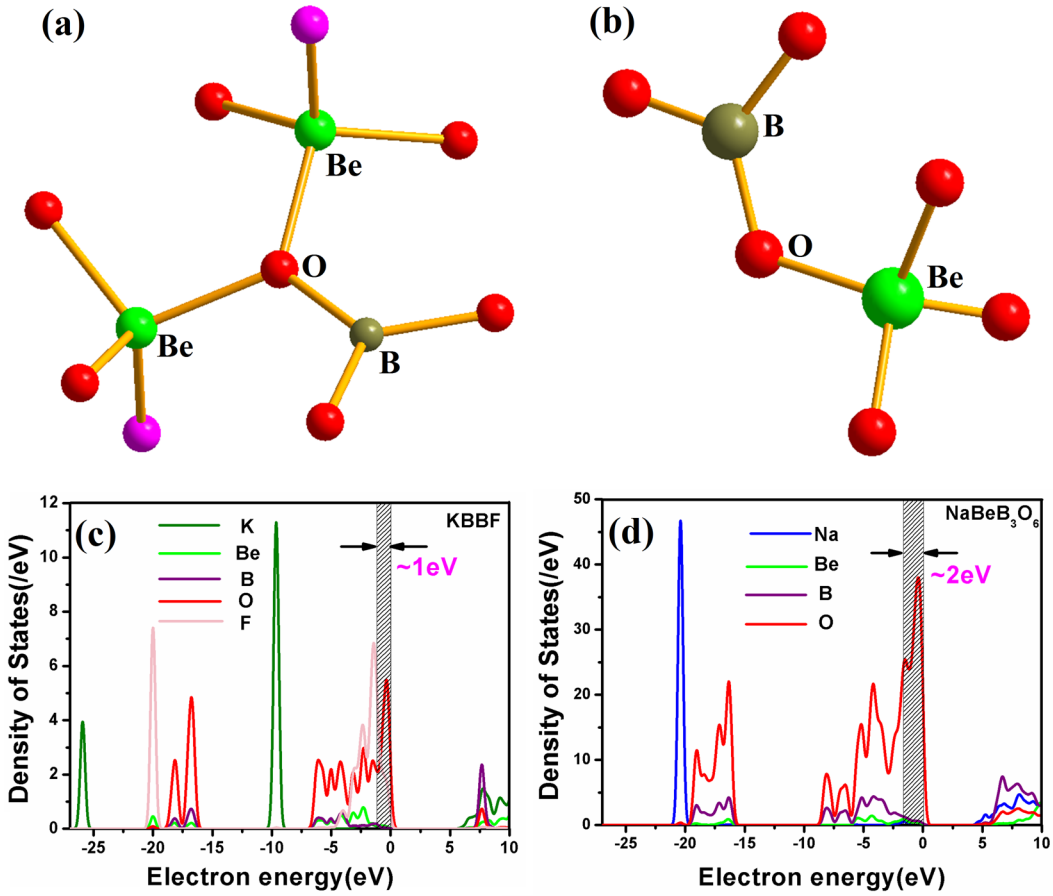

Figure 2. Comparison of the coordinated enviornments around oxygen atoms in (a) KBBF and (b) $NaBeB_3O_6$ and the density of states for (c) KBBF and (d) $NaBeB_3O_6$.

COMPUTATIONAL DETAILS

The lattice parameters and atomic positions used in the computation are directly obtained from the experimental determination. Our further tests show that the optical properties obtained from the experimental and geometrically optimized crystal structures did not exhibit significant deviation (see Table S1).

The first-principles calculations are carried out by CASTEP,[33] a plane-wave pseudopotential total energy package based on DFT.[34] The electronic exchange−correlation functionals developed by Ceperley, Alder, Perdew, and Zunger (CA-PZ) in local density approximation (LDA)[35,36] form are adopted. In the optimized pseudopotentials,[37] the Li $2s^1$, Na $2s^22p^63s^1$, K $3s^23p^64s^1$, Rb $4s^24p^65s^1$, Cs $5s^25p^66s^1$, Ca $3s^23p^64s^2$, Sr $4s^24p^65s^1$, Be $2s^2$, B $2s^22p^1$, O $2s^22p^4$, and F $2s^22p^5$ are treated as valence electrons. The kinetic energy cutoff of 900 eV and dense Monkhorst-pack[38] k-point mesh spanning less than 0.05 $Å^{-1}$ in the Brillouin zones are chosen. Our tests showed that the above computational parameters and methodology are sufficiently accurate for the current study.

It is well known that the energy band gaps calculated by the LDA method are smaller than the measured values, due to the discontinuity of exchange−correlation energy. The scissor operators[39] are adopted to shift all the conduction bands to match the calculated band gaps with the measured values. For the crystals whose experimental band gaps have not been accurately determined, the "measured" band gaps are predicted by the hybridized PBE0 functionals.[40] This is because the PBE0 band gaps match the available experimental values for UV borates very well (the relative error is less than 5%).[41] On the basis of the scissor-corrected electron band structure, the imaginary part of the dielectric function is calculated according to the electron transition from the valence bands (VB) to conduction bands (CB). Consequently, the real part of the dielectric function is obtained by the Kramers−Kronig

DOI: 10.1021/acsphotonics.5b00248
ACS Photonics 2015, 2, 1183−1191

Table 2. Calculated and Measured SHG Effect of the Investigated Beryllium Borates[a]

	SHG coefficients (calcd)	powder SHG[b]	
		calcd	exptl
$KBe_2BO_3F_2$	d_{11} = 0.45 pm/V		d_{11} = 0.49 pm/V[53]
$RbBe_2BO_3F_2$	d_{11} = 0.44 pm/V		d_{11} = 0.50 pm/V[53]
$CsBe_2BO_3F_2$	d_{11} = 0.42 pm/V		d_{11} = 0.50 pm/V[53]
$NaCaBe_2B_2O_6F$	$d_{26} = d_{12}$ = 0.10 pm/V, $d_{31} = d_{15}$ = 0.27 pm/V $d_{32} = d_{24}$ = −0.17 pm/V, $d_{35} = d_{13}$ = 0.16 pm/V d_{11} = 0.27 pm/V, d_{33} = 0.04 pm/V	0.8 KDP	0.6 KDP[25]
$NaSr_3Be_3B_3O_9F$	$d_{31} = d_{15}$ = −0.03 pm/V d_{22} = 0.88 pm/V, d_{33} = −0.37 pm/V	1.2 KDP	2 KDP[23]
$NaBeB_3O_6$	$d_{31} = d_{15}$ = −0.54 pm/V $d_{32} = d_{24}$ = 0.75 pm/V, d_{33} = −0.34 pm/V	0.6 LBO (1.6 KDP)	0.9 LBO[27] (2.4 KDP)
$Na_2Cs_2Be_6B_5O_{15}$	$d_{14} = d_{25} = d_{36}$ = −0.28 pm/V, $d_{21} = d_{16}$ = −0.14 pm/V $d_{34} = d_{23}$ = −0.34 pm/V, d_{22} = 0.58 pm/V	0.5 LBO (1.3 KDP)	0.7 LBO[26] (1.8 KDP)
β-$KBe_2B_3O_7$	$d_{31} = d_{15}$ = 0.09 pm/V $d_{32} = d_{24}$ = 0.31 pm/V, d_{33} = −0.38 pm/V	0.3 LBO (0.8 KDP)	0.6 LBO (1.6 KDP)
γ-$KBe_2B_3O_7$	$d_{14} = d_{25} = d_{36}$ = 0.13 pm/V, $d_{21} = d_{16}$ = −0.28 pm/V $d_{34} = d_{23}$ = −0.08 pm/V, d_{22} = 0.32 pm/V	0.4 LBO (1.1 KDP)	0.6 LBO[27] (1.6 KDP)
$RbBe_2B_3O_7$	$d_{31} = d_{15}$ = −0.08 pm/V $d_{32} = d_{24}$ = −0.28 pm/V, d_{33} = 0.36 pm/V	0.4 LBO (1.1 KDP)	0.6 LBO[27] (1.6 KDP)
$Na_2Be_4B_4O_{11}$	$d_{14} = d_{25} = d_{36}$ = −0.01 pm/V, $d_{21} = d_{16}$ = −0.02 pm/V $d_{26} = d_{12}$ = 0.42 pm/V, $d_{31} = d_{15}$ = 0.12 pm/V $d_{32} = d_{24}$ = −0.17 pm/V, $d_{34} = d_{23}$ = 0.00 pm/V $d_{35} = d_{13}$ = −0.08 pm/V, d_{11} = −0.44 pm/V d_{22} = 0.01 pm/V, d_{33} = 0.07 pm/V	1.1 KDP	1.1 KDP[24]
$LiNa_5Be_{12}B_{12}O_{33}$	d_{11} = −0.42 pm/V, $d_{26} = d_{12}$ = 0.50 pm/V $d_{31} = d_{15}$ = 0.12 pm/V, $d_{32} = d_{24}$ = −0.19 pm/V $d_{35} = d_{13}$ = −0.09 pm/V, d_{33} = 0.08 pm/V	1.2 KDP	1.2 KDP[24]

[a]The experimentally measured powder SHG effect in the table has been transferred from the multiple relation of the powder SHG signal to that of powder SHG coefficients by a square root. [b]Theoretical powder SHG coefficients are 0.33 and 0.87 pm/V for KDP (KH_2PO_4) and LBO (LiB_3O_5), respectively.

transform, and the refractive index is determined.[42] After obtaining the refractive indices at variable wavelengths the refractive-index dispersive curves are fitted by the least-squares method, and the shortest SHG wavelength is determined according to the phase-matching condition.[43] The SHG coefficients are calculated by the formula developed by our groups,[30,44] and the powder SHG effect is determined using the Kurtz and Perry method.[45] Our previous studies have demonstrated that the calculated optical properties by these first-principles methods are in very good agreement with the available experimental results.[30]

RESULTS AND DISCUSSION

Short-Wavelength Absorption Edges (or Energy Band Gaps). Good transmission in the DUV region is the primary condition for the DUV NLO crystal. The calculated and experimental short-wavelength absorption edges λ_{cutoff} of the alkali and/or alkaline earth beryllium borates are listed in Table 1. Although the LDA energy band gaps are much less than the experimental values, the values calculated by hybridized PBE0 functionals are in very good agreement with the available experimental values, confirming the feasibility of PBE0 functionals in predicting the energy band gaps E_g of the studied crystals. Both the PBE0 calculations and experiments demonstrate that the absorption edges of all the studied crystals are less than 200 nm (E_g > 6.2 eV) and satisfy the basic optical transmission requirement for the DUV NLO crystal.

It is interesting that the absorption edges of the KBBF family crystals are located at about 150 nm ($E_g \approx$ 8.3 eV), while those of the other crystals are all longer than 170 nm (E_g < 7.3 eV). This difference mainly originates from the different atomic coordination around the oxygen anions. In the KBBF family crystals each oxygen anion in $(BO_3)^{3-}$ groups is connected with two neighboring beryllium cations (see Figure 2a), while in the other crystals there always exists an oxygen anion in the $(BO_3)^{3-}$ groups that connects with one beryllium cation only (e.g., $NaBeB_3O_6$ in Figure 2b). Therefore, the nonbonding states on oxygen that determine the energy band gaps for these crystals[46,47] are more effectively eliminated in the former crystals since the valence electrons on the beryllium atoms are very easily attracted by the oxygen atoms due to the small electronegativity of Be. The partial densities of states (PDOS) displayed in Figure 2c and d clearly show that the nonbonding states span about 1 eV in KBBF, while spanning more than 2 eV in other crystals (e.g., in $NaBeB_3O_6$). Thus, the KBBF family has a very large energy band gap.

SHG Effect. Table 2 listed the calculated and experimental SHG effects for the alkali and/or alkaline earth beryllium borate crystals. The negative value of the SHG coefficient means that the induced second-order susceptibility is in the opposite direction from the external photoelectric field. Clearly, good agreement between the calculated and available measured SHG effects is obtained, confirming the validity of the plane-wave pseudopotential method to the present purpose. It is shown that all these crystals exhibit an SHG effect on the order of KDP (~0.39 pm/V), thus reaching the essential requirement for the DUV NLO crystal as well.

DOI: 10.1021/acsphotonics.5b00248
ACS Photonics 2015, 2, 1183−1191

Table 3. Calculated Refractive Index (n_x, n_y, and n_z), Birefringence at 400 nm (Δn), and Shortest SHG Phase-Matching Wavelength (λ_{PM}) in the Studied Beryllium Borate Crystals[a]

		n_x	n_y	n_z	Δn	λ_{PM} (nm)
I	KBBF[20]	1.501 (1.489)	1.501 (1.489)	1.437 (1.411)	0.064 (0.078)	174 (161)
	RBBF[21]	1.527 (1.420)	1.527 (1.420)	1.466 (1.498)	0.061 (0.078)	187 (170)
	CBBF[54]	1.552 (1.522)	1.552 (1.522)	1.495 (1.458)	0.057 (0.064)	202 (201)
	$NaCaBe_2B_2O_6F$	1.674	1.666	1.616	0.058	245
	$NaSr_3Be_3B_3O_9F_4$[55]	1.616 (1.617)	1.616 (1.617)	1.561 (1.555)	0.055 (0.061)	239 (233)
II	$NaBeB_3O_6$	1.565	1.638	1.558	0.080	226
	γ-$KBe_2B_3O_7$	1.562	1.621	1.581	0.059	243
	$Na_2Cs_2Be_6B_5O_{15}$	1.590	1.599	1.605	0.015	452
III	β-$KBe_2B_3O_7$	1.606	1.588	1.568	0.038	290
	$RbBe_2B_3O_7$	1.616	1.604	1.578	0.038	284
	$Na_2Be_4B_4O_{11}$	1.592	1.610	1.563	0.047	256
	$LiNa_5Be_{12}B_{12}O_{33}$	1.593	1.608	1.562	0.046	258

[a]The values in parentheses are the measured value.

The anionic group theory[48] and our previous first-principles studies[30,49] have demonstrated that the NLO effect of UV borates mainly arises from the geometrical superposition of the microscopic second-order susceptibility in the B−O anionic groups, especially in the $(BO_3)^{3-}$ groups. Namely, the magnitudes of the SHG response in these crystals almost depend on the spatial orientation and density of the $(BO_3)^{3-}$ groups: (i) in $NaCaBe_2B_2O_6F$ the $(BO_3)^{3-}$ groups are aligned in a nearly antiparallel orientation (shown in Figure S1a), which is an unfavorable pattern for generating a large SHG effect, so it exhibits the smallest SHG effect in all studied crystals. (ii) In the crystal structures of the KBBF family, $Na_2Cs_2Be_6B_5O_{15}$, β-$KBe_2B_3O_7$, γ-$KBe_2B_3O_7$, $RbBe_2B_3O_7$, $Na_2Be_4B_4O_{11}$, and $LiNa_5Be_{12}B_{12}O_{33}$ (the example for γ-$KBe_2B_3O_7$ is shown in Figure S1b), the $(BO_3)^{3-}$ groups are in the same orientation in the $(Be_2BO_3F_2)_\infty$ layers for the KBBF family and in the $(Be_2BO_5)_\infty$ layers for the other crystals, while the B−O groups outside the layers are in a nearly centrosymmetric arrangement and contribute almost nothing to the NLO response. These crystals possess a similar SHG effect (about 1 × KDP), and the small fluctuation in magnitude is mainly attributed to the different spatial density of the $(BO_3)^{3-}$ groups. (iii) In $NaSr_3Be_3B_3O_9F_4$ and $NaBeB_3O_6$ (for the example for $NaSr_3Be_3B_3O_9F_4$ see Figure S1c) the basic building block tri-six-membered rings $[Be_3B_3O_{12}F]^{10-}$ and $[Be_2B_3O_{11}]^{9-}$ make the $(BO_3)^{3-}$ groups in nearly the same plane normal to the c-axis with almost parallel orientation and very large spatial density, leading to the largest SHG response in these two crystals compared with the other alkali and/or alkaline earth beryllium borates.

Optical Birefringence. Table 3 lists the calculated optical birefringence in the alkali and/or alkaline earth beryllium borates (the refractive-index dispersions are listed in Table S2), which match well with the available experimental data. It is shown that, except KBBF, RBBF, and $NaBeB_3O_6$, the birefringence in the other crystals is smaller than 0.07 at the wavelength of 400 nm, indicating that they cannot satisfy the birefringence condition for the DUV SHG crystal. Similar to the SHG effects, the optical birefringence is also mainly contributed from the planar arranged $(BO_3)^{3-}$ anionic groups, but not sensitive to the exact orientation of the $(BO_3)^{3-}$ groups, because it is almost optically isotropic within the BO_3 plane.[50] Accordingly, all the studied crystals can be catalogued into three structural types according to the arrangement of $(BO_3)^{3-}$ groups (also see Figure 1): the $(BO_3)^{3-}$ planes arranged in a nearly coplanar pattern (type-I, including the KBBF family, $NaCaBe_2B_2O_6F$, and $NaSr_3Be_3B_3O_9F$), in a coaxial pattern (type-II, including $NaBeB_3O_6$, γ-$KBe_2B_3O_7$, and $Na_2Cs_2Be_6B_5O_{15}$), and in the other inclined patterns (type-III, including β-$KBe_2B_3O_7$, $RbBe_2B_3O_7$, $Na_2Be_4B_4O_{11}$, and $LiNa_5Be_{12}B_{12}O_{33}$). In general, the type-I crystals have the largest birefringence, while the type-III crystals have the smallest birefringence, resulting from the coplanar and inclined arrangement of $(BO_3)^{3-}$ groups, respectively, as demonstrated in the previous studies.[30,31]

The situation of the type-II crystals is complicated. The birefringence of this type of crystal exhibits a large variation. $NaBeB_3O_6$ possesses the largest birefringence ($\Delta n \approx 0.08$), while that of $Na_2Cs_2Be_6B_5O_{15}$ is the smallest ($\Delta n \approx 0.015$) in all crystals. This observation actually disobeys the conclusion recently obtained by Bian et al. that the coaxially aligned $(BO_3)^{3-}$ group must lead to large optical anisotropy.[51] In order to clarify this point, we made an in-depth investigation on the relationship between the arrangement of $(BO_3)^{3-}$ groups and birefringence in this type of crystal. It is known that the refractive index is determined by the superposition of the microscopic first-order polarizability of constituent ions or groups along the macroscopic optical axis (x, y and z), and the birefringence is the difference between the maximum and minimum refractive indices ($n_{max} - n_{min}$). Analogous to the SHG effect, the birefringence in UV beryllium borates mainly originates from the planar $(BO_3)^{3-}$ groups.[30] In a $(BO_3)^{3-}$ group the maximum and minimum microscopic first-order polarizabilities (p_{max} and p_{min}) are parallel and perpendicular to the B−O plane, respectively, owing to the strong optical anisotropy from the π-conjugated orbitals.[48] Our calculations using the Gaussian03 package[52] (at the B3LYP/6-311+G* level) also confirm that the microscopic polarizabilities parallel and perpendicular to a $(BO_3)^{3-}$ group are 37.11 and 11.60 × 10^{-40} C*m^2/V, respectively. As the $(BO_3)^{3-}$ groups are all parallel to an optical axis in a crystal, the refractive index along this axis must be maximal (n_{max}), and the minimal refractive index (n_{min}) depends on the orientation of the (BO_3) planes with respect to the other two optical axes. Taking $NaBeB_3O_6$ as an example, Figure 3a shows the geometry pattern of $(BO_3)^{3-}$ groups in the unit cell. Since all B−O planes are parallel to the y-axis, the maximum refractive index contributed from the $(BO_3)^{3-}$ groups must be along this axis, i.e., $n_y = n_{max} \propto 1/V \sum_i p_{max}$, and the other two refractive indices are

DOI: 10.1021/acsphotonics.5b00248
ACS Photonics 2015, 2, 1183−1191

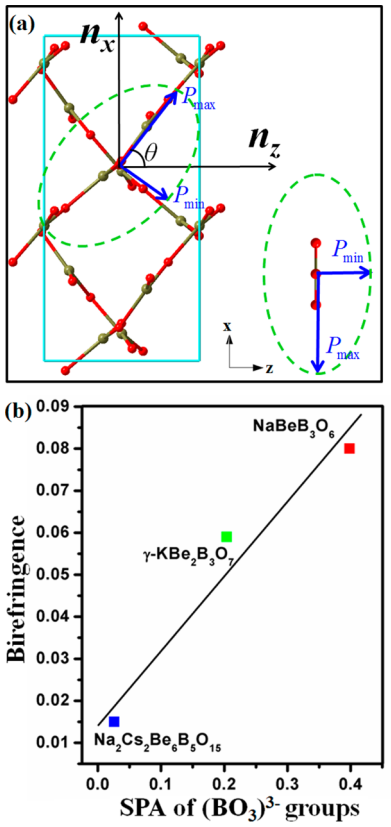

Figure 3. (a) Contribution of the polarizability in a $(BO_3)^{3-}$ group to the macroscopic refractive index n_x and n_z in $NaBeB_3O_6$. P_{max} and P_{min} are the maximum and minimum microscopic polarizabilities of (BO_3) groups, which are parallel and perpendicular to the B−O plane, respectively. (b) Positive relationship between SPA of $(BO_3)^{3-}$ groups and birefringence in type-II crystals.

$$n_x \propto \frac{1}{V}\sum_i \sqrt{\frac{P_{max}^2 P_{min}^2}{P_{min}^2 \sin^2\theta_i + P_{max}^2 \cos^2\theta_i}} \text{ and } n_z \propto \frac{1}{V}\sum_i \sqrt{\frac{P_{max}^2 P_{min}^2}{P_{min}^2 \cos^2\theta_i + P_{max}^2 \sin^2\theta_i}}$$

where θ_i is the angle between the ith $(BO_3)^{3-}$ group and the z-axis and V is the volume of the unit cell, which also determine the spatial density of the $(BO_3)^{3-}$ groups. The smaller one of n_x and n_z is the minimum refractive index (n_z is smaller in $NaBeB_3O_6$). Thus, the birefringence in $NaBeB_3O_6$ is determined by the sum of the difference between the intersection lengths of the y-axis and z-axis on the polarizability ellipsoid (the sum of polarizability anisotropy, SPA) for all $(BO_3)^{3-}$ groups. Using a similar method, the SPA of the $(BO_3)^{3-}$ groups in γ-$KBe_2B_3O_7$ and $Na_2Cs_2Be_6B_5O_{15}$ can be obtained (see Table S3). Figure 3b shows the strong linear relation between the SPA for all $(BO_3)^{3-}$ groups and the birefringence in the three type-II crystals. Therefore, the diversity of birefringence values in this type of structure can be explained: their birefringence depends not only on the coaxial arrangement but also on the detailed orientation and spatial density of the $(BO_3)^{3-}$ groups.

Refractive-Index Dispersion. Actually, the birefringence itself is not enough to determine the phase-matching condition for the shortest SHG wavelength of a crystal. As clearly shown in Table 3, the birefringence of $NaBeB_3O_6$ is the largest ($\Delta n \approx$ 0.08 at 400 nm) among all known alkali and/or alkaline earth beryllium borates and seems to satisfy the commonly accepted criterion for the birefringence for the DUV NLO crystal.[17] However, our calculations based on the phase-matching condition reveal that its shortest SHG wavelength cannot reach the DUV region, but is just located at 226 nm. As a comparison, the birefringence in the KBBF family crystals is smaller, but their shortest SHG wavelengths are much blue-shifted to the DUV region. Upon noticing this phenomenon, we highlight that the refractive-index dispersion must be accounted for by determining the SHG phase-matching capability for a DUV NLO crystal, which was normally ignored in previous studies.

Generally speaking, the SHG phase-matching condition can be achieved when the following requirement is satisfied: $n_{max}(\lambda) > n_{min}(\lambda/2)$, where $n_{max}(\lambda)$ and $n_{min}(\lambda/2)$ are the largest and smallest refractive indices at the fundamental and SHG wavelengths, respectively.[43] Figure 4a and b display the refractive-index dispersion in $NaBeB_3O_6$ and KBBF, respectively. It is explicitly shown that in $NaBeB_3O_6$ $n_{max}(400\text{ nm}) < n_{min}(200\text{ nm})$, while in KBBF $n_{max}(400\text{ nm}) > n_{min}(200\text{ nm})$. Thus, the SHG phase-matching condition in the DUV region cannot be achieved in the former, but can be satisfied in the latter crystal. The weak DUV phase-matching capability in $NaBeB_3O_6$ originates from the larger refractive-index dispersion than KBBF, especially in the spectral region below 400 nm. For instance, in $NaBeB_3O_6$ the refractive-index n_y increases by 0.14, while in KBBF the n_e increases by only 0.05, as the wavelengths are varied from 400 to 200 nm. Therefore, the consideration of the role of refractive-index dispersion is crucial to determine the shortest SHG wavelength for a DUV crystal, since the spectral region below 200 nm is close to the short-wavelength absorption edge and the refractive-index dispersion is usually very large.

The large difference in refractive-index dispersion between KBBF and $NaBeB_3O_6$ originates from their structural difference. KBBF possesses a 2D atomic structure in which the interaction between the $(Be_2BO_3F_2)_\infty$ layers is very weak; thus the electronic transitions are nearly limited in the single layers. As a comparison, in $NaBeB_3O_6$, the basic building blocks, the nearly coplanar double six-membered $(Be_2B_3O_{11})^{9-}$ rings, are connected with each other in a cross manner and form a dense 3D framework; hence the electronic transitions are quite delocalized. This electronic characteristic difference is also exhibited in the density of states of KBBF and $NaBeB_3O_6$ (see Figure 4c): the low part of the CB in $NaBeB_3O_6$ appears much more diffusive than that in KBBF, showing the larger hybridization among the excited energy states in the former crystal. The more delocalized electronic transitions result in a stronger optical absorption (Figure 4d) and a larger refractive-index dispersion in $NaBeB_3O_6$ (a detailed discussion on a large refractive index resulting from large absorption is shown in Sect. S1). From the above analysis, one may conclude that the layer structures, compared with the coaxial structures, should be more favorable for the DUV SHG crystals. Meanwhile, the above mechanism is also demonstrated in the KBBF family of crystals. The order of hybridization degree of the excited energy states in the KBBF family of crystals is KBBF < RBBF < CBBF (Figure S2), and consequently, both the absorption and refractive-index dispersion are also in the order KBBF < RBBF < CBBF, as the wavelength is varied from 400 to 200 nm (Figure S3).

DOI: 10.1021/acsphotonics.5b00248
ACS Photonics 2015, 2, 1183−1191

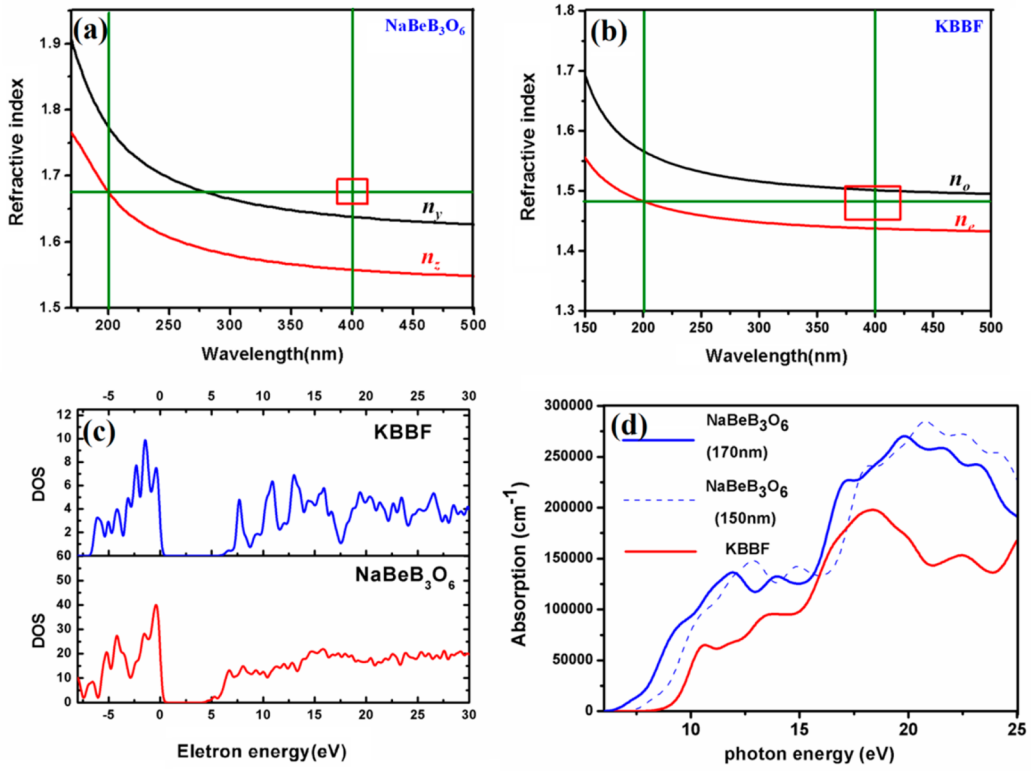

Figure 4. Phase-matching capabilities for (a) $NaBeB_3O_6$ and (b) KBBF at 400 nm. The minimum refractive index at 200 nm located between the minimun and maxium refractive index at 400 nm indicates the fulfillment of the requirement of the phase-matching condition. (c) Comparison of the density of state near the forbidden bands of $NaBeB_3O_6$ and KBBF. (d) Calculated absorption curves of $NaBeB_3O_6$ and KBBF. The curve labeled 150 nm is the absorption spectrum for the (hypothetical) $NaBeB_3O_6$ having the short-wavelength absorption edge of KBBF, which also exhibits a larger absorption in $NaBeB_3O_6$ compared with KBBF even without considering the energy band gap.

CONCLUSION

Using first-principles calculations, the key optical properties for the DUV NLO performance in the known alkali and/or alkaline earth beryllium borates were determined. The calculated results match the available experimental results very well. It was highlighted that the refractive-index dispersion, in addition to the energy band gap, SHG effect, and birefringence, is a crucial factor for determining the DUV SHG capability of a crystal. On the basis of the conditions required for a good DUV SHG material, we predict that in all studied beryllium borates KBBF and RBBF are the only two crystals that can practically produce coherent light with a wavelength below 200 nm by direct SHG; CBBF, $NaCaBe_2B_2O_6F$, $NaSr_3Be_3B_3O_9F_4$, $NaBeB_3O_6$, $Na_2Be_4B_4O_{11}$, γ-$KBe_2B_3O_7$, and $LiNa_5Be_{12}B_{12}O_{33}$ may have promising applications of the fourth-harmonic generation for the Nd:YAG laser (at 266 nm); β-$KBe_2B_3O_7$ and $RbBe_2B_3O_7$ may be useful for the generation of the 355 nm laser; and $Na_2Cs_2Be_6B_5O_{15}$ can be used only in visible lasers.

We also investigated the structural and electronic mechanisms of the optical properties in these materials. The SHG response and birefringence both originate from the arrangements of the $(BO_3)^{3-}$ anionic groups, not only the construction geometry but also the spatial density. In particular, the large birefringence can result from either the layer arrangement or the coaxial arrangement of the B−O groups. Nevertheless, the coaxial patterns of the atomic structures would result in the delocalization of the electronic transitions and then lead to the large refractive-index dispersion, which may hinder the achievement of phase-matching conditions in the DUV region. Therefore, the crystals with layer structures would be more favorable for the DUV coherent light production by SHG. We believe that the evaluation of the structure−property relationship in this work has significant implications in the exploration of new DUV NLO crystals with good performances.

ASSOCIATED CONTENT

Supporting Information

The Supporting Information is available free of charge on the ACS Publications website at DOI: 10.1021/acsphotonics.5b00248.

Additional tables, figures and section. (PDF)

AUTHOR INFORMATION

Corresponding Authors

*E-mail: shichao-wang@northwestern.edu.
*E-mail: zslin@mail.ipc.ac.cn.

Notes

The authors declare no competing financial interest.

ACKNOWLEDGMENTS

This work was supported by the NSF of China (Grant 11174297), China "863" project (Grant 2015AA034203), and China "973" project (Grant 2011CB922204). The authors acknowledge the useful discussion with Dr. Ran He and Dr. Wenjiao Yao.

DOI: 10.1021/acsphotonics.5b00248
ACS Photonics 2015, 2, 1183−1191

REFERENCES

(1) Herman, P. R.; Marjoribanks, R. S.; Oettl, A.; Chen, K.; Konovalov, I.; Ness, S. Laser Shaping of Photonic Materials: Deep-Ultraviolet and Ultrafast Lasers. *Appl. Surf. Sci.* **2000**, *154*, 577−586.

(2) Witte, S.; Zinkstok, R. T.; Ubachs, W.; Hogervorst, W.; Eikema, K. S. E. Deep-Ultraviolet Quantum Interference Metrology with Ultrashort Laser Pulses. *Science* **2005**, *307*, 400−403.

(3) Balakrishnan, G.; Hu, Y.; Nielsen, S. B.; Spiro, T. G. Tunable KHZ Deep Ultraviolet (193-210 nm) Laser for Raman Applications. *Appl. Spectrosc.* **2005**, *59*, 776−781.

(4) Meng, J. Q.; et al. Coexistence of Fermi Arcs and Fermi Pockets in a High-T_C Copper Oxide Superconductor. *Nature* **2009**, *462*, 335−338.

(5) Mou, D. X.; et al. Distinct Fermi Surface Topology and Nodeless Superconducting Gap in a $(Tl_{0.58}Rb_{0.42})Fe_{1.72}Se_2$ Superconductor. *Phys. Rev. Lett.* **2011**, *106*, 107001.

(6) Cyranoski, D. Materials Science: China's Crystal Cache. *Nature* **2009**, *457*, 953−955.

(7) Czeranowsky, C.; Heumann, E.; Huber, G. All-Solid-State Continuous-Wave Frequency-Doubled Nd: YAG-BIBO Laser with 2.8-W Output Power at 473 nm. *Opt. Lett.* **2003**, *28*, 432−434.

(8) Kanai, T.; Kanda, T.; Sekikawa, T.; Watanabe, S.; Togashi, T.; Chen, C. T.; Zhang, C. Q.; Xu, Z. Y.; Wang, J. Y. Generation of Vacuum-Ultraviolet Light Below 160nm in a KBBF Crystal by the Fifth Harmonic of a Single-Mode Ti: Sapphire Laser. *J. Opt. Soc. Am. B* **2004**, *21*, 370−375.

(9) Borsutzky, A.; Brunger, R.; Huang, C.; Wallenstein, R. Harmonic and Sum-Frequency Generation of Pulsed Laser-Radiation in BBO, LBO, and KDP. *Appl. Phys. B: Photophys. Laser Chem.* **1991**, *52*, 55−62.

(10) McMillen, C. D.; Kolis, J. W. Hydrothermal Crystal Growth of $ABe_2BO_3F_2$ (a = K, Rb, Cs, Tl) NLO Crystals. *J. Cryst. Growth* **2008**, *310*, 2033−2038.

(11) Yu, P.; Wu, L.-M.; Zhou, L.-J.; Chen, L. Deep-Ultraviolet Nonlinear Optical Crystals: $Ba_3P_3O_{10}X$ (X = Cl, Br). *J. Am. Chem. Soc.* **2014**, *136*, 480−487.

(12) Wu, H.; Yu, H.; Pan, S.; Huang, Z.; Yang, Z.; Su, X.; Poeppelmeier, K. R. $Cs_2B_4SiO_9$: A Deep-Ultraviolet Nonlinear Optical Crystal. *Angew. Chem., Int. Ed.* **2013**, *52*, 3406−3410.

(13) Zhao, S.; Gong, P.; Luo, S.; Liu, S.; Li, L.; Asghar, M. A.; Khan, T.; Hong, M.; Lin, Z.; Luo, J. Beryllium-Free $Rb_3Al_3B_3O_{10}F$ with Reinforced Inter Layer Bonding as a Deep-Ultraviolet Nonlinear Optical Crystal. *J. Am. Chem. Soc.* **2015**, *137*, 2207−2210.

(14) Wu, H.; Yu, H.; Yang, Z.; Hou, X.; Su, X.; Pan, S.; Poeppelmeier, K. R.; Rondinelli, J. M. Designing a Deep-Ultraviolet Nonlinear Optical Material with a Large Second Harmonic Generation Response. *J. Am. Chem. Soc.* **2013**, *135*, 4215−4218.

(15) Zou, G.; Ye, N.; Huang, L.; Lin, X. Alkaline-Alkaline Earth Fluoride Carbonate Crystals $ABCO_3F$ (A = K, Rb, Cs; B = Ca, Sr, Ba) as Nonlinear Optical Materials. *J. Am. Chem. Soc.* **2011**, *133*, 20001−20007.

(16) Chen, C. T.; Ye, N.; Lin, J.; Jiang, J.; Zeng, W. R.; Wu, B. C. Computer-Assisted Search for Nonlinear Optical Crystals. *Adv. Mater.* **1999**, *11*, 1071−1078.

(17) Yao, W.; He, R.; Wang, X.; Lin, Z.; Chen, C. Analysis of Deep-UV Nonlinear Optical Borates: Approaching the End. *Adv. Opt. Mater.* **2014**, *2*, 411−417.

(18) Kang, L.; Ramo, D. M.; Lin, Z.; Bristowe, P. D.; Qin, J.; Chen, C. First Principles Selection and Design of Mid-IR Nonlinear Optical Halide Crystals. *J. Mater. Chem. C* **2013**, *1*, 7363−7370.

(19) Chen, C. T.; Wang, G. L.; Wang, X. Y.; Xu, Z. Y. Deep-Uv Nonlinear Optical Crystal $KBe_2BO_3F_2$-Discovery, Growth, Optical Properties and Applications. *Appl. Phys. B: Lasers Opt.* **2009**, *97*, 9−25.

(20) Wu, B. C.; Tang, D. Y.; Ye, N.; Chen, C. T. Linear and Nonlinear Optical Properties of the $KBe_2BO_3F_2$ (KBBF) Crystal. *Opt. Mater.* **1996**, *5*, 105−109.

(21) Chen, C. T.; Luo, S. Y.; Wang, X. Y.; Wang, G. L.; Wen, X. H.; Wu, H. X.; Zhang, X.; Xu, Z. Y.; Deep, U. V. Nonlinear Optical Crystal: $RbBe_2(BO_3)F_2$. *J. Opt. Soc. Am. B* **2009**, *26*, 1519−1525.

(22) Huang, H.; Chen, C.; Wang, X.; Zhu, Y.; Wang, G.; Zhang, X.; Wang, L.; Yao, J. Ultraviolet Nonlinear Optical Crystal: $CsBe_2BO_3F_2$. *J. Opt. Soc. Am. B* **2011**, *28*, 2186−2190.

(23) Huang, H. W.; Yao, J. Y.; Lin, Z. S.; Wang, X. Y.; He, R.; Yao, W. J.; Zhai, N. X.; Chen, C. T. $NaSr_3Be_3B_3O_9F_4$: A Promising Deep-Ultraviolet Nonlinear Optical Material Resulting from the Cooperative Alignment of the $(Be_3B_3O_{12}F)^{10-}$ Anionic Group. *Angew. Chem., Int. Ed.* **2011**, *50*, 9141−9144.

(24) Huang, H. W.; Liu, L. J.; Jin, S. F.; Yao, W. J.; Zhang, Y. H.; Chen, C. T. Deep-Ultraviolet Nonlinear Optical Materials: $Na_2Be_4B_4O_{11}$ and $LiNa_5Be_{12}B_{12}O_{33}$. *J. Am. Chem. Soc.* **2013**, *135*, 18319−18322.

(25) Huang, H. W.; Yao, J. Y.; Lin, Z.; Wang, X. Y.; He, R.; Yao, W. J.; Zhai, N. X.; Chen, C. T. Molecular Engineering Design to Resolve the Layering Habit and Polymorphism Problems in Deep UV NLO Crystals: New Structures in MM′ $Be_2B_2O_6F$ (M = Na, M′ = Ca; M= K, M′ = Ca, Sr). *Chem. Mater.* **2011**, *23*, 5457−5463.

(26) Wang, S. C.; Ye, N. $Na_2CsBe_6B_5O_{15}$: An Alkaline Beryllium Borate as a Deep-UV Nonlinear Optical Crystal. *J. Am. Chem. Soc.* **2011**, *133*, 11458−11461.

(27) Wang, S. C.; Ye, N.; Li, W.; Zhao, D. Alkaline Beryllium Borate $NaBeB_3O_6$ and $ABe_2B_3O_7$ (A = K, Rb) as UV Nonlinear Optical Crystals. *J. Am. Chem. Soc.* **2010**, *132*, 8779−8786.

(28) Chen, C. T.; Wang, Y. B.; Wu, B. C.; Wu, K. C.; Zeng, W. L.; Yu, L. H. Design and Synthesis of an Ultraviolet-Transparent Nonlinear-Optical Crystal $Sr_2Be_2B_2O_7$. *Nature* **1995**, *373*, 322−324.

(29) Meng, X. Y.; Wen, X. H.; Liu, G. L. Structure and Stacking Faults in $Sr_2Be_2B_2O_7$ Crystal. *J. Korean Phys. Soc.* **2008**, *52*, 1277−1280.

(30) Lin, Z. S.; Jiang, X. X.; Kang, L.; Gong, P. F.; Luo, S. Y.; Lee, M. H. First-Principles Materials Applications and Design of Nonlinear Optical Crystals. *J. Phys. D: Appl. Phys.* **2014**, *47*, 253001.

(31) Jiang, X.; Kang, L.; Luo, S.; Gong, P.; Lee, M.-H.; Lin, Z. Development of Nonlinear Optical Materials Promoted by Density Functional Theory Simulations. *Int. J. Mod. Phys. B* **2014**, *28*, 1430018.

(32) Zhang, M.; et al. Linear and Nonlinear Optical Properties of $K_3B_6O_{10}Br$ Single Crystal: Experiment and Calculation. *J. Phys. Chem. C* **2014**, *118*, 11849−11856.

(33) Clark, S. J.; Segall, M. D.; Pickard, C. J.; Hasnip, P. J.; Probert, M. J.; Refson, K.; Payne, M. C. First Principles Methods Using Castep. *Z. Kristallogr.* **2005**, *220*, 567−570.

(34) Kohn, W.; Sham, L. J. Self-Consistent Equations Including Exchange and Correlation Effects. *Phys. Rev.* **1965**, *140*, 1133.

(35) Perdew, J. P.; Zunger, A. Self-Interaction Correction to Density-Functional Approximations for Many-Electron Systems. *Phys. Rev. B: Condens. Matter Mater. Phys.* **1981**, *23*, 5048−5079.

(36) Ceperley, D. M.; Alder, B. J. Ground-State of the Electron-Gas by a Stochastic Method. *Phys. Rev. Lett.* **1980**, *45*, 566−569.

(37) Rappe, A. M.; Rabe, K. M.; Kaxiras, E.; Joannopoulos, J. D. Optimized Pseudopotentials. *Phys. Rev. B: Condens. Matter Mater. Phys.* **1990**, *41*, 1227−1230.

(38) Monkhorst, H. J.; Pack, J. D. Special Points for Brillouin-Zone Integrations. *Phys. Rev. B* **1976**, *13*, 5188−5192.

(39) Godby, R. W.; Schluter, M.; Sham, L. J. Self-Energy Operators and Exchange-Correlation Potentials in Semiconductors. *Phys. Rev. B: Condens. Matter Mater. Phys.* **1988**, *37*, 10159−10175.

(40) Adamo, C.; Barone, V. Toward Reliable Density Functional Methods without Adjustable Parameters: The Pbe0Model. *J. Chem. Phys.* **1999**, *110*, 6158−6170.

(41) Lin, Z. S.; Kang, L.; Zheng, T.; He, R.; Huang, H.; Chen, C. T. Strategy for the Optical Property Studies in Ultraviolet Nonlinear Optical Crystals from Density Functional Theory. *Comput. Mater. Sci.* **2012**, *60*, 99−104.

(42) Palik, E. D. *Handbook of Optical Constants of Solids*; Academic Press: New York, 1985.

(43) Boyd, R. W. *Nonlinear Optics*; Academic Press, 2003.

(44) Lin, J.; Lee, M. H.; Liu, Z. P.; Chen, C. T.; Pickard, C. J. Mechanism for Linear and Nonlinear Optical Effects in Beta-BaB_2O_4

DOI: 10.1021/acsphotonics.5b00248
ACS Photonics 2015, 2, 1183−1191

Crystals. *Phys. Rev. B: Condens. Matter Mater. Phys.* **1999**, *60*, 13380−13389.
(45) Kurtz, S. K.; Perry, T. T. A Powder Technique for Evaluation of Nonlinear Optical Materials. *J. Appl. Phys.* **1968**, *39*, 3798−3813.
(46) He, R.; Huang, H. W.; Kang, L.; Yao, W. J.; Jiang, X. X.; Lin, Z. S.; Qin, J. G.; Chen, C. T. Bandgaps in the Deep Ultraviolet Borate Crystals: Prediction and Improvement. *Appl. Phys. Lett.* **2013**, *102*, 231904.
(47) He, R.; Lin, Z. S.; Zheng, T.; Huang, H.; Chen, C. T. Energy Band Gap Engineering in Borate Ultraviolet Nonlinear Optical Crystals: *Ab Initio* Studies. *J. Phys.: Condens. Matter* **2012**, *24*, 145503.
(48) Chen, C.; Lin, Z.; Wang, Z. The Development of New Borate-Based Uv Nonlinear Optical Crystals. *Appl. Phys. B: Lasers Opt.* **2005**, *80*, 1−25.
(49) Lin, Z. S.; Lin, J.; Wang, Z. Z.; Wu, Y. C.; Ye, N.; Chen, C. T.; Li, R. K. Theoretical Calculations and Predictions of the Nonlinear Optical Coefficients of Borate Crystals. *J. Phys.: Condens. Matter* **2001**, *13*, R369−R384.
(50) Chen, C.; Sasaki, T.; Li, R.; Wu, Y.; Lin, Z.; Mori, Y.; Hu, Z.; Wang, J.; Aka, G.; Yoshimura, M.; Kaneda, Y. *Nonlinear Optical Borate Crystals-Princples and Applications*; Wiley-VCH: New York, 2012.
(51) Bian, Q.; Yang, Z.; Dong, L.; Pan, S.; Zhang, H.; Wu, H.; Yu, H.; Zhao, W.; Jing, Q. First Principle Assisted Prediction of the Birefringence Values of Functional Inorganic Borate Materials. *J. Phys. Chem. C* **2014**, *118*, 25651−25657.
(52) Frisch, M. J.; Trucks, G. W.; Schlegel, H. B.; Scuseria, G. E.; Robb, M. A.; Cheeseman, J. R.; Montgomery, J. A., Jr.; Vreven, T.; Kudin, K. N.; Burant, J. C.; Millam, J. M.; Iyengar, S. S.; Tomasi, J.; Barone, V.; Mennucci, B.; Cossi, M.; Scalmani, G.; Rega, N.; Petersson, G. A.; Nakatsuji, H.; Hada, M.; Ehara, M.; Toyota, K.; Fukuda, R.; Hasegawa, J.; Ishida, M.; Nakajima, T.; Honda, Y.; Kitao, O.; Nakai, H.; Klene, M.; Li, X.; Knox, J. E.; Hratchian, H. P.; Cross, J. B.; Bakken, V.; Adamo, C.; Jaramillo, J.; Gomperts, R.; Stratmann, R. E.; Yazyev, O.; Austin, A. J.; Cammi, R.; Pomelli, C.; Ochterski, J. W.; Ayala, P. Y.; Morokuma, K.; Voth, G. A.; Salvador, P.; Dannenberg, J. J.; Zakrzewski, V. G.; Dapprich, S.; Daniels, A. D.; Strain, M. C.; Farkas, O.; Malick, D. K.; Rabuck, A. D.; Raghavachari, K.; Foresman, J. B.; Ortiz, J. V.; Cui, Q.; Baboul, A. G.; Clifford, S.; Cioslowski, J.; Stefanov, B. B.; Liu, G.; Liashenko, A.; Piskorz, P.; Komaromi, I.; Martin, R. L.; Fox, D. J.; Keith, T.; Al-Laham, M. A.; Peng, C. Y.; Nanayakkara, A.; Challacombe, M.; Gill, P. M. W.; Johnson, B.; Chen, W.; Wong, M. W.; Gonzalez, C.; Pople, J. A. *Gaussian03*, Revisions C.01, C.02, D.02, and E.01; Gaussian, Inc.: Wallingford, CT, 2004.
(53) Kang, L.; Luo, S.; Huang, H.; Zheng, T.; Lin, Z. S.; Chen, C. T. Ab Initio Studies on the Optical Effects in the Deep Ultraviolet Nonlinear Optical Crystals of the $KBe_2BO_3F_2$ Family. *J. Phys.: Condens. Matter* **2012**, *24*, 335503.
(54) Huang, H. W.; Chen, C. T.; Wang, X. Y.; Zhu, Y.; Wang, G. L.; Zhang, X.; Wang, L. R.; Yao, J. Y. Ultraviolet Nonlinear Optical Crystal: $CsBe_2BO_3F_2$. *J. Opt. Soc. Am. B* **2011**, *28*, 2186−2190.
(55) Wang, X.; Liu, L.; Wang, X.; Bai, L.; Chen, C. Growth and Optical Properties of the Novel Nonlinear Optical Crystal $NaSr_3Be_3B_3O_9F_4$. *CrystEngComm* **2015**, *17*, 925−929.

DOI: 10.1021/acsphotonics.5b00248
ACS Photonics 2015, 2, 1183−1191